Geometry of the momentum space: From wire networks to quivers and monopoles

RALPH M. KAUFMANN
SERGEI KHLEBNIKOV
BIRGIT WEHEFRITZ–KAUFMANN

A new nano–material in the form of a double gyroid has motivated us to study (non)–commutative C^* geometry of periodic wire networks and the associated graph Hamiltonians. Here we present the general abstract framework, which is given by certain quiver representations, with special attention to the original case of the gyroid as well as related cases, such as graphene. In these geometric situations, the non–commutativity is introduced by a constant magnetic field and the theory splits into two pieces: commutative and non–commutative, both of which are governed by a C^* geometry.

In the non–commutative case, we can use tools such as K–theory to make statements about the band structure. In the commutative case, we give geometric and algebraic methods to study band intersections; these methods come from singularity theory and representation theory. We also provide new tools in the study, using K–theory and Chern classes. The latter can be computed using Berry connection in the momentum space. This brings monopole charges and issues of topological stability into the picture.

1 Introduction

Recently, a new nano–material in the form of a double gyroid has been synthesized [1]. It is based on a thickened triply-periodic minimal surface, whose complement consists of two non-intersecting channels. These can be filled with conducting or semiconducting materials [1] to function as nanowire networks with potentially useful electronic properties [2]. The nontrivial topology of such a network has motivated our study of its commutative and non–commutative geometry [3]. Following Bellissard and Connes [4, 5, 6], we proceed by indentifying the relevant C^*–algebra, which in our case is spanned by the symmetries and the tight-binding (Harper) Hamiltonian of the skeletal graph obtained as a deformation retract of the channel; we call it the Bellissard-Harper algebra. This approach leads to an effective geometry described by a family

of finite dimensional Hamiltonians and their spectra; the latter determine the band structure of the original nanostructured solid in the tight-binding approximation. By placing the material into an external constant magnetic field the geometry is rendered noncommutative.

In this paper, we generalize that setup to further noncommutative geometries obtained via certain quiver representations. We also adapt the techniques of [7] and [8] to this more general situation. In particular, in the commutative case, we get a classification of singularities in the spectrum—the band intersections. The simplest of these is a conical intersection of two bands, commonly referred to as a Dirac point. We give analytic tools to compute locations and properties of the singular points.

In the general framework above, we also give a new interpretation of the Berry phase phenomenon [9] in terms of K–theory and Chern–classes generalizing the observations of Thouless *et al.* (TKNN) [10] and Simon [11]. These concepts include topological charges in various guises: scalar, K–theoretic and cohomological. When the parameter space is three-dimensional, isolated conical degeneracies are magnetic monopoles in the parameter space [9]. In the present case, the parameters are components of the crystal momentum $\mathbf{k}$; their number equals the dimensionality of the original periodic structure. Thus, in three spatial dimensions—the case of the gyroid—Dirac points are monopoles in the momentum space and, as we will see, are stable with respect to small deformations of the graph Hamiltonian. Furthermore, using foliations, we consider a slicing technique which leads to an effective numerical tool for finding singular points in the spectrum, generalizing the method used for this purpose in [12]. This technique has been implemented in [13] and corroborates the topological stability of the gyroid's Dirac points. This stability is not a common characteristic of all Dirac points: those of graphene, which is described by the honeycomb lattice, do not exhibit this property, see e.g. [14][1]. This fact has an elegant and short explanation in our approach. We expect that this analysis will contribute to understanding of potential applications of gyroid-based nanomaterials, as well as to the theory of three-dimensional generalizations of the quantum Hall effect, along the lines of [15]. In two dimensions, the TKNN equations for generalized Dirac–Harper operators have been worked out in [16]. Analyses of higher-dimensional situations are contained in [17, 18, 19, 20, 21].

Even without going to complete generality provided by quiver representations, our approach to studying wire networks is not restricted to the gyroid system and applies to any embedded periodic wire network in $\mathbb{R}^n$. We have already used it to study more examples, namely, Bravais lattices, the honeycomb lattice and two other triply

[1]That article also explores deformation direction where the Dirac points do stay stable.

periodic surfaces and their wire networks, the primitive cubic (P surface) and the diamond (D surface). We refer to these as the geometric examples. We recall some results here and include a new consideration of the topological charges. In these cases the noncommutative geometry is given by a subalgebra of a matrix algebra with coefficients in the noncommutative torus. Here the parameters of the torus correspond to the B–field that the material is subjected to.

One surprising fact is that some properties of the non–commutative situation are similar to the situation without a magnetic field, and there is evidence for duality between these two situations. The duality concerns the degenerate subspaces of the torus that appears as the relevant moduli space in both cases. In the commutative case, i.e. in the absence of a magnetic field, the torus is the base for the family of Hamiltonians and the requsite subspace is where the spectrum of the Hamiltonian has degeneracies. In the noncommutative case, the same torus parameterizes the B–field and the locus of degeneracy is that of those values of B where the Bellissard–Harper algebra is not the full matrix algebra.

The paper is organized as follows: we start with a description of the material and its underlying geometry in Chapter 2. Here the geometry is reduced to that of the skeletal graph—the deformation retract of a channel component of the complement to the triply periodic surface. We also introduce other related geometries which we consider in parallel. These are the honeycomb lattice underlying graphene, and the P and D surfaces, which are the other triply periodic self–symmetric surfaces. Chapter 3 describes the mathematical model we work with. This includes the Harper Hamiltonian and the relevant Hilbert space and C^* algebra, the Bellissard–Harper algebra. We discuss the C^* geometry in Chapter 4. This includes our analysis of the Berry connection, topological charges and stability of the singular points as well as a slicing method to detect singular points or monopoles. Chapter 5 contains our results about degeneracies in the spectrum of the Harper Hamiltonian in the commutative case using singularity and representation theories. In Chapter 6 we summarize the results of our analysis for the cases mentioned above including the new results about the topological charges. We finish this chapter and the paper with a conjecture about a commutative/non–commutative duality and remarks about approaching it.

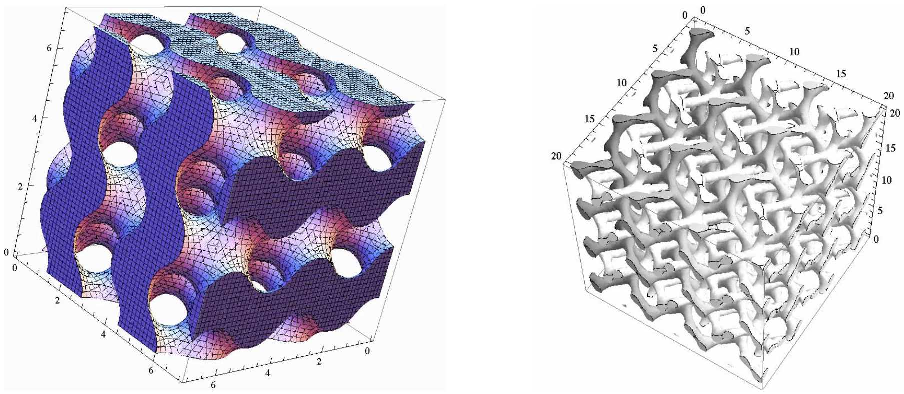

Figure 1: The fat gyroid surface W (left) and the two channel systems C_+ and C_- (right)

2 The Double Gyroid (DG) and Related Geometries and Material

2.1 The Geometry

The gyroid is a triply periodic constant mean curvature surface that is embedded in $\mathbb{R}^3$ [22]. Figure 1 shows a picture of the gyroid. It was discovered in 1970 by Alan Schoen [23]. A single gyroid has symmetry group $I4_132$ in Hermann-Maguin notation. Here the letter I stands for bcc. The gyroid surface can be visualized by using the level surface approximation [24]

$$L_t : \sin x \cos y + \sin y \cos z + \sin z \cos x = t \tag{1}$$

In nature the single gyroid was observed as an interface for di–block co–polymers [25]. The **double gyroid** consists of two mutually non–intersecting embedded gyroids. Its symmetry group is $Ia\bar{3}d$ where the extra symmetry comes from interchanging the two gyroids. It also has a level surface approximation which is given by the above expression (1) with L_w and L_{-w} for $0 \leq w < \sqrt{2}$. The picture on the left hand side of Figure 1 is actually a double gyroid or a “thick" surface.

Let us fix some notation. We will denote by $S = S_1 \amalg S_2$ the double gyroid surface. Its complement $C = \mathbb{R}^3 \setminus S$ has three connected components, which we will call C_+, C_- and W. W can be thought of as a “thickened” (fat) surface which we will refer to as DG wall. There is a deformation retract of W onto a single gyroid.

There are also two channel systems C_+ and C_-, shown in Figure 1. These channels form Y-junctions where three channels meet under a 120 degree angle. Each of

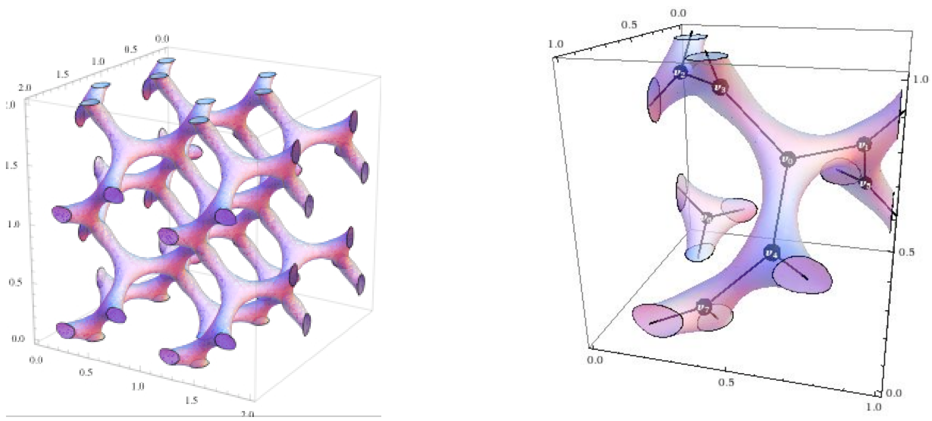

Figure 2: One of the two channels (left) and its skeletal graph in the unit cell (right)

these channel systems can be deformation retracted to a skeletal graph $\Gamma_{\pm}$. We will concentrate on one of these channels and its skeletal graph Γ_{+}, shown in Figure 2.

2.2 The Material and Production

A solid-state double gyroid can be synthesized by self-assembly at the nanoscale, as demonstrated by Urade et al. [1]. The first step is production of a nanoporous silica film with the structure of unidirectionally cotracted double gyroid (DG) with lattice constant of about 18 nm. The pores in the structure can then be filled with other materials to form nanowires. Fabrication of platinum DG nanowires by electrodeposition has been demonstrated in [1], where it has also been mentioned that the process can be used for other metals or semiconductors.

2.3 Related Geometries: the P and D surfaces

There are two other triply periodic self–dual and symmetric CMC surfaces- the cubic (P) and the diamond (D) network. They are shown in Figure 3 together with their wire networks obtained in the same way as for the gyroid. Here we summarize the results from [26].

The P surface has a complement which has two connected components each of which can be retracted to the simple cubical graph whose vertices are the integer lattice $\mathbb{Z}^3 \subset \mathbb{R}^3$. The translational group is $\mathbb{Z}^3$ in this embedding, so it reduces to the case of a Bravais lattice.

The D surface has a complement consisting of two channels each of which can be retracted to the diamond lattice $\Gamma_\diamond$. The diamond lattice is given by two copies of the fcc lattice, where the second fcc is the shift by $\frac{1}{4}(1,1,1)$ of the standard fcc lattice, see Figure 3. The edges are nearest neighbor edges. The symmetry group is $Fd\bar{3}m$.

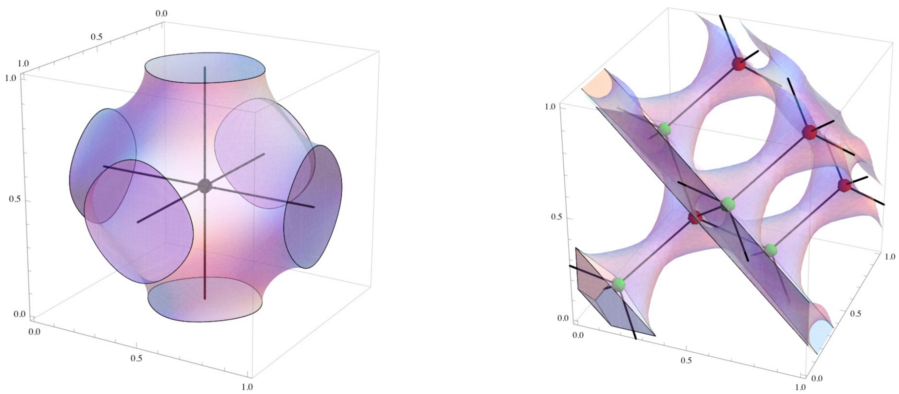

Figure 3: The cubic (P) (left) and the diamond (D) wire network (right)

2.4 Graphene

Graphene consists of one-atom thick planar sheets of carbon atoms that are densely packed in a honeycomb crystal lattice. This two–dimensional material has attracted much interest recently, partially because of the existence of Dirac points where excitations show a linear dispersion relation. Its electronic properties are described by a Harper Hamiltonian: see the review [27] and references therein. Here we will reproduce some of the known facts, such as the Dirac points using our non–commutative geometry machine.

3 Mathematical Model and Generalization: Graphs and Groupoid Representation

3.1 Discrete model and Harper Hamiltonian

We will now describe how to obtain the Harper Hamiltonian for any given graph $\Gamma \in \mathbb{R}^n$ with a given maximal translation group $L \simeq \mathbb{Z}^n$ [28]. We will start with the commutative case without an external field, and then progress to non–commutative

case where the graph is placed in a constant external magnetic field. The mathematical set–up we will describe below can be understood in terms of Weyl quantization and Peierls substitution in physics [29]. Without the magnetic field the Harper Hamiltonian is given by translations, but in the presence of a magnetic field all translations turn into magnetic translations or Wannier operators, which cease to commute with each other.

Mathematically the discretization by the above process yields the Hilbert space $\mathscr{H} = \ell^2(V(\Gamma))$, where $V(\Gamma)$ are the vertices of Γ, and a projective representation of the translation group L as well as an operator H, the Harper Hamiltonian. Concretely, the elements l of L act on the functions Ψ via the usual translations $T_l : T_l\psi(l') = \Psi(l-l')$.

3.2 Quotient Graph and Harper Hamiltonian

In general, given a embedded graph $\Gamma \in \mathbb{R}^n$, with a given maximal translation group $L \simeq \mathbb{Z}^n$, we consider the quotient graph $\bar{\Gamma} := \Gamma/L$ and the projection $\pi : \Gamma \to \bar{\Gamma}$. The quotient graphs for our four main examples are given in Figure 4.

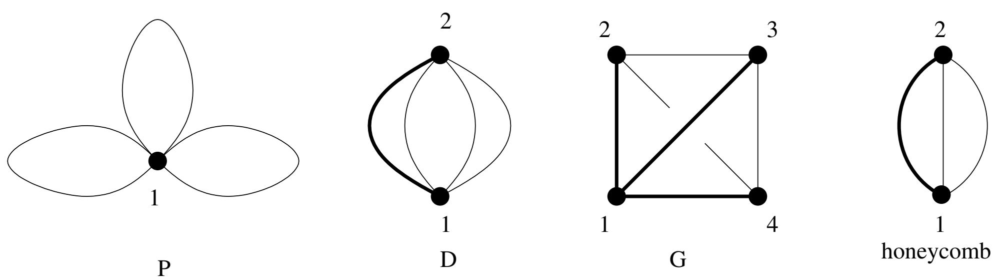

Figure 4: The quotient graphs of the P,D,G surfaces and the honeycomb lattice, together with a spanning tree and an order of the vertices.

The vertices of this graph are in 1–1 correspondence with vertices or sites of Γ in a fundamental cell. We can think of the graph $\bar{\Gamma}$ as embedded into $T^n = \mathbb{R}^n/\mathbb{Z}^n$. Each edge e of $\bar{\Gamma}$ lifts to a pair of edge vectors $\vec{e}, \overleftarrow{e} = -\vec{e}$ where the underlying line segment is any lift of e to Γ. This is well defined since any two lifts differ by a translation.

To each vertex $v \in \bar{\Gamma}$ we can associate the Hilbert space $\mathscr{H}_v := \ell^2(\pi^{-1}(v))$. Then the whole Hilbert space $\mathscr{H}$ decomposes as

(2) $$\mathscr{H} = \bigoplus_{v \text{ vertex of } \bar{\Gamma}} \mathscr{H}_v$$

Since all the $\mathscr{H}_v$ are separable Hilbert spaces, they are all isomorphic.

The Harper Hamiltonian is then given as follows. For each edge e between two vertices v and w of $\bar{\Gamma}$ let $T_{\vec{e}}$ be the translation operator from $\mathscr{H}_w \to \mathscr{H}_v$. This extends to an operator $\hat{T}_{\vec{e}}$ on $\mathscr{H}$ via $\hat{T}_{\vec{e}} = i_{\bar{v}} T_{\vec{e}} P_{\bar{w}}$ where $i_{\bar{v}} : \mathscr{H}_{\bar{v}} \to \mathscr{H}$ is the inclusion and $P_{\bar{w}} : \mathscr{H} \to \mathscr{H}_{\bar{w}}$ is the projection.

The Harper Hamiltonian is

$$H = \sum_{e \in E} \hat{T}_{\vec{e}} + \hat{T}_{-\vec{e}} \tag{3}$$

3.3 Harper Hamiltonian in the presence of a magnetic field

Adding a constant magnetic field requires a slightly different definition of the Harper Hamiltonian. We will use projective translation operators whose commutators include the fluxes of the magnetic field as follows: We define a 2–cocycle $\alpha_B \in Z^2(T, U(1))$ by a two–form Θ. Such a two–form is given by a skew symmetric matrix $\hat{\Theta}$ with $\Theta = \hat{\Theta}_{ij} dx_i \wedge dx_j$. We let $B = 2\pi\Theta$ where B is the norm of the magnetic field. In this way we obtain a two–cocycle $\alpha_B \in Z^2(\mathbb{R}^n, U(1))$: $\alpha_B(u,v) = \exp(\frac{i}{2}B(u,v))$.

We define magnetic translations by starting from A, which is a potential for B (on $\mathbb{R}^n$). The magnetic translation partial isometry is now acting on a wave function as

$$U_{l'}\psi(l) = e^{-i\int_l^{(l-l')} A}\,\psi(l-l')$$

The magnetic Harper operator is defined as

$$H = \sum_{e \text{ edges of } \bar{\Gamma}} U_{\vec{e}} + U_{\overleftarrow{e}} \tag{4}$$

3.4 Generalization: Groupoid and quiver representations

In the setting above, which we call the geometric examples, we have distilled the following data: a finite graph $\bar{\Gamma}$, the translational groups L and a projective representation of it on $\mathscr{H} = \bigoplus \mathscr{H}_v$ and finally the Hamiltonian H.

We will now explore the possibility of obtaining such data from a more general setup. There are two ways to do this: in terms of groupoids or in terms of quivers.

3.4.1 Groupoid representation

Recall that a groupoid is a category whose morphisms are all invertible. A representation of a groupoid is a functor from this category into a linear category. In our case this will be the category of separable Hilbert spaces which is the full subcategory of the category of vector spaces whose objects are separable Hilbert spaces.

A graph $\bar{\Gamma}$ (here $\bar{\Gamma}$ need not be finite) determines a groupoid $\mathcal{G}$ as follows. The objects are the vertices of Γ. The morphisms are *generated* by the edges. That is for each oriented edge between v and w there is one generator $\phi_{\overrightarrow{e}}$ in $Hom(v,w)$. The morphisms in this category are then the composable words in the $\phi_{\overrightarrow{e}}$ where composable means that the source of a letter is the target of the predecessor, with the relations that

$$\phi_{\overrightarrow{e}}\phi_{\overleftarrow{e}} = id_v \in Hom(v,v), \text{ the identity element} \tag{5}$$

What this means is that the morphisms are the paths on Γ up to homotopy, with the constant path yielding the identity.

A groupoid representation of $\mathcal{G}$ it in separable Hilbert spaces then assigns to each vertex v of $\bar{\Gamma}$ a separable Hilbert space $\mathscr{H}_v$ and to each oriented edge $\overrightarrow{e}$ from v to w a morphism $\Phi_{\overrightarrow{e}} \in Hom(\mathscr{H}_v, \mathscr{H}_w)$ with the relation that $\Phi_{\overrightarrow{e}}\Phi_{\overleftarrow{e}} = id_{\mathscr{H}_v}$.

The groupoid representation is unitary if all the $\Phi_{\overrightarrow{e}}$ are.

Remark 3.1 Notice that there is an involution $*$ on the morphisms, by transposing the word and reversing the orientation of each letter. So we can only look at involutive functors, that is functors which send $*$ to $\dagger$, which guarantees that the representation is unitary.

3.4.2 Quiver representation

There is a way to formulate this in quiver language. Given a graph $\bar{\Gamma}$ and an arbitrary choice of directions for the edges determines a quiver. Now one can construct the double of the quiver, where each oriented edge is doubled with reverse orientation. If we started from a graph, this means that each unoriented edge e is replaced by the two oriented edges $\overrightarrow{e}$ and $\overleftarrow{e}$. Now the double of the quiver is independent of the original choice of orientation. It also has an involution on $*$ the set of its edges which is given by reversing orientation. The quiver representations we are looking at are those where $*$ goes to $\dagger$.

3.4.3 Hamiltonian of the representation

Just as above we define

$$H := \sum_{e \in E(\bar{\Gamma})} \rho(\overrightarrow{e}) + \rho(\overleftarrow{e}) : \mathscr{H} \to \mathscr{H}$$

3.4.4 Representation of $\pi_1(\bar{\Gamma})$

If we fix a vertex v_0 of Γ the groupoid representation naturally gives a representation of $\pi_1(\bar{\Gamma})$ as follows. Fix a set of generators of $\pi_1(\bar{\Gamma}) = \mathbb{F}_{1-\chi(\bar{\Gamma})}$ is the free group in $1-\chi$ generators. Each such generator g_i is a directed simple loop on the graph which is given by a sequence of directed edges $\overrightarrow{e}_{1i}, \dots, \overrightarrow{e}_{n_i i}$. Then $\rho(g_i) = \rho(\overrightarrow{e}_{1i}) \circ \cdots \circ \rho(\overrightarrow{e}_{n_i i})$ gives a representation of $\pi_1(\bar{\Gamma}, v_0)$ on $\mathscr{H}_{v_0}$.

Definition 3.2 We will denote the algebra generated by $\rho(\pi_1)$ by $\mathscr{T}$. We say the ρ is maximal if the generators of π_1 map to linearly independent operators and that ρ is of torus type if $\mathscr{T} = \mathbb{T}_\Theta$.

If ρ is of torus type then ρ is a projective representation of $H_1(\bar{\Gamma})$, the Abelianization of π_1. These are of a special type, namely those whose co–cycle is given by a constant B field as discussed in [3].

In the geometric situation of Chapters 3.1–3.3, maximality is equivalent to the fact that the translational symmetry group is maximal.

3.4.5 Spanning trees

If we pick a rooted spanning tree of $\bar{\Gamma}$ then we get isomorphisms $\phi_{0v} : \mathscr{H}_{v_0} \simeq \mathscr{H}_v$ by using ρ and concatenation along the unique shortest path of oriented edges from v_0 to v in the spanning tree. Let $\Phi = \bigoplus_v \phi_{v0} : \mathscr{H}_{v_0}^{|V|} \to \mathscr{H}$ then this isomorphisms yields a representation $\tilde{\rho}$ on $\mathscr{H}_{v_0}^{|V|}$ via pullback.

Likewise ϕ_{v0} induces an isomorphism of $\pi_1(\bar{\Gamma}, v)$ and $\pi_1(\bar{\Gamma}, v_0)$. Using this identification, we get an representation $\hat{\rho}$ of $\mathscr{T}$ on $\mathscr{H}$ and via pull-back with Φ on $\mathscr{H}_{v_0}^{|V|}$.

A rooted spanning tree (τ, v_0) also gives rise to one more bijection. This is between a set of (symmetric) generators of π_1 and the edges *not* in the spanning tree. The bijection is as follows.

If $\vec{e}$ is a directed edge from v to w then there is a generator $g_{\vec{e}}$ which is given by the following path of ordered edges: (1) the unique shortest path in τ from v_0 to v (2) $\vec{e}$ and (3) the unique shortest path in τ from w to v_0. It is clear that $g_{\vec{e}} = g^{-1}_{\overleftarrow{e}}$. By contracting the spanning tree, we see that this is indeed a set of symmetric but otherwise independent generators.

For convenience, we set $g_{\vec{e}} = 1$ if $e \in \tau$.

3.4.6 Generalized Bellissard-Harper algebra

Given a groupoid representation in separable Hilbert spaces of a finite graph $\bar{\Gamma}$ we call the C^* algebra generated by the operators H and $\mathscr{T}$ via $\hat{\rho}$ on $\mathscr{H}$ the Bellissard–Harper algebra of the pair $(\bar{\Gamma}, \rho)$ and denote it by $\mathscr{B}$.

This general set gives the generalization of one of the results of [3].

Theorem 3.3 *Any choice of spanning tree together with an order on the vertices gives rise to a faithful matrix representation of $\mathscr{B}$ in $M_{|V|}(\mathscr{T})$.*

Proof This follows from the fact that under Φ, $\rho(\vec{e})$ gets transformed to the matrix entry $\rho(g_{\vec{e}})$ between the copies of $\mathscr{H}_{v_0}$ corresponding to $\mathscr{H}_v$ and $\mathscr{H}_w$ under Φ. Enumerating these vertices yields a matrix. □

In the following given a rooted spanning tree τ we will only choose orders $<$ such that the root is the first element. The resulting matrix Hamiltonian will be denoted by $H_{\tau,<}$.

4 C^*–geometry

4.1 Non–commutative case

The non–commutative geometry of such a quiver representation in general and the one stemming from the geometric situation in particular is that of $\mathscr{B}$.

Just like in [3, 26] one can now ask the question whether or not $\mathscr{B}$ is isomorphic to the full matrix algebra and hence Morita equivalent to $\mathscr{T}$ itself. In the geometric case $\mathscr{T} = \mathbb{T}_\Theta$ is generically simple and led to the expectation —which we proved in [3]— that generically $\mathscr{B} = M_{|V|}(\mathbb{T}_\Theta)$. This of course need not be the case in general.

It stands to reason that other more complicated physical phenomena could be described by such algebras.

It actually turns out that in the geometric examples not only is the algebra indeed the full matrix algebra at irrational parameter values, but that there are even only finitely many or a dimension–1 subset of rational matrix parameters Θ, where $\mathscr{B} \subsetneq M_k(\mathbb{T}_\Theta)$.

Theorem 4.1 *[3, 26] For the geometric cases of the G surface and the honeycomb lattice the Bellissard–Harper algebra is the full matrix algebra except at finitely many values of Θ given in Chapter 6. For the P surface and all Bravais lattices $\mathscr{B} = \mathscr{T} = M_1(\mathscr{T})$. For the D surface, the set of values of Θ for which $\mathscr{B} \subsetneq M_2(\mathbb{T}_\Theta)$ is given by 6 one dimensional families and finitely many special points (also listed in Chapter 6). If $\mathscr{B}_\Theta$ is the full matrix algebra then it is Morita equivalent to $\mathbb{T}_\Theta$.*

Remark 4.2 Note that except for the P and general Bravais case, these families above give examples of continuos variations of algebras whose K–theory does not vary continuously.

4.1.1 K–theory labeling

One application of the non–commutative approach is gap labeling by K–theory. If the Hamiltonian H has spectrum bounded from below, then each gap in the spectrum gives rise to a projector $P_{<E}$ onto the Eigenspaces with Eigenvalues less than any fixed value E in the gap, see e.g. [4]. The gap labeling then associates the K–theory class of $P_{<E}$ to the gap.

By the above result, via the inclusion $\mathscr{B} \hookrightarrow M_k(\mathscr{T})$ the projector $P_{<E}$ also gives rise to a K–theory class in $K(M_k(\mathscr{T})) \simeq K(\mathscr{T})$. Using this embedding, one can deduce analogues of the famous Hofstadter Butterfly.

Theorem 4.3 *If $(\bar{\Gamma}, \rho)$ is toric non–degenerate, then the Hamiltonian H as an operator on $\mathscr{H}$ has only finitely many gaps if the magnetic field is rational in the sense that the matrix Θ is rational.*

4.2 Commutative case

If $\mathscr{B}$ is commutative, for instance if $\Theta = 0$ in the geometric situation, then by the Gel'fand–Naimark theorem, there is a compact[2] Hausdorff space X, such that

[2] $\mathscr{B}$ is unital

$\mathscr{B} \simeq C^*(X)$. The points of X can be thought of as characters, i.e. C^*–homomorphisms $\chi : \mathscr{B} \to \mathbb{C}$. More precisely these characters are in bijection with the maximal ideals of $\mathscr{B}$ which are the points. If we wish to make this distinction, we write p_χ for the point of X corresponding to the character χ and vice–versa χ_p for the character corresponding to p.

Likewise there is a space T which corresponds to the C^*–algebra $\mathscr{T}$. In the geometric case $T = T^n = \mathbb{R}^n/L$.

As usual the correspondence between the algebra of functions and the spaces is contravariant. This means that the inclusion $\hat{\rho} : \mathscr{T} \to \mathscr{B}$ gives rise to a morphism $X \to T$. If (ρ, Γ) is maximal, then $\mathscr{T} \to \mathscr{B}$ is injective and hence $X \to T$ is surjective.

Furthermore let us consider the algebra $\mathscr{T}^n$ given by the direct sum of n copies of $\mathscr{T}$. The space corresponding to this algebra is simply $T \amalg \cdots \amalg T$ n–times.

Since after choosing an order and a rooted spanning tree $\mathscr{B} \subset M_{|V|}(\mathscr{T})$, we can lift any character χ of $\mathscr{T}$ to a C^*-homomorphism: $\hat{\chi} : M_{|V|}(\mathscr{T}) \to M_{|V|}(\mathbb{C})$ of $\mathscr{B}$ by applying χ to each entry.

Definition 4.4 We call a point χ of T degenerate if $\hat{\chi}(H)$ has less than $|V|$ distinct Eigenvalues.

Repeating the proof of [3] we arrive at the following

Theorem 4.5 *If $(\rho, \bar{\Gamma})$ is maximal the map $\pi : X \to T$ is ramified over the degenerate points and furthermore X is the quotient of the trivial cover T^n where the identifications are made in the fibers over degenerate points and moreover these correspond to the degeneracies of H over these points.*

In other words X can be thought of as the spectrum of the family of Hamiltonians $H(p) = \chi_p(H)$ parameterized over T.

The key ingredient is the image of H under the map $\mathscr{B} \to \mathscr{T}^n$

$$H \mapsto \sum_i \lambda_i e_i \tag{6}$$

where e_i are the idempotents corresponding to the i–th component and λ_i is the i–th Eigenvalue.

4.2.1 Bundles, K-theoretic and Cohomology Valued Charges

Let T_{deg} be the subset of degenerate points on T and let $X_{\mathrm{deg}} = \pi^{-1}(T_{\mathrm{deg}})$ be the closed possibly singular locus of X. Then the restriction $\pi : X_0 := X \setminus X_{\mathrm{deg}} \to T_0 := T \setminus T_{\mathrm{deg}}$ is the trivial k–fold cover. On this restriction the $C(X \setminus X_{\mathrm{deg}})$ contains pairwise orthogonal projections P_i such that $H = \sum_i P_i$. Each of these P_i defines a rank 1 sub–bundle L_i of the trivial bundle $X_0 \times \mathbb{C}$ which is the Eigenbundle corresponding to the Eigenvalue λ_i. The projector or equivalently the bundle L_i defines an element in K–theory $[L_i] \in K(T_0)$. We will continue with the geometric interpretation of line bundles and K–theory here, although in forthcoming analysis we will concentrate on the C^* version of K–theory in oder to move to a non–commutative setup.

We call the classes $[L_i]$ the K–theoretic charges and the associated Chern classes $\beta_i := c_1(L_i) \in H^2(T_0)$ the cohomological charges. We also let $C = \bigoplus_i L_i$, and $[C] \in K(T_0)$ be its class in K–theory. Finally we define the polynomial invariant $Q_c(t_i) = \prod_i (1 + t_i \beta_i) \in H^{\mathrm{ev}}(T_0)[t_i]$. This class contains all the cohomological information of the L_i and C.

Remark 4.6 If $H(t)$ is not Hermitian, we also need the condition $\pi_1(T_0) = 0$ in order for the characteristic polynomial to be irreducible over $C(T_0)$ which is necessary to define the P_i.

Remark 4.7 We assumed that the Hamiltonians are generically non–degenerate. It is sufficient to assume that the ranks of the Eigenbundles are generically constant. In this case, we have vector bundles V_i and total Chern classes $c(V_i)$.

4.3 Berry connection, topological charge and slicing

One can try to get numerical information about Q_c and the β_i by pairing them with appropriate homology classes. For this it is easier to assume that we are dealing with oriented manifolds. If we furthermore have a differentiable structure, we know that we can evaluate Chern classes by using Chern–Weil theory.

Of course the charges are trivial if T_0 has vanishing second cohomology (e.g. if T_0 is 2–connected). In that case the Chern classes β_i vanish and the line bundles $[L_i]$ are trivializable. This is the case in some examples, notably the honeycomb. The effect is that the line bundles are trivializable and the associated points of degeneracy are not topologically stable, see §4.6.

The two–torus or the two–sphere do however have non–vanishing H^2 and thus are prime candidates to detect first Chern classes.

Furthermore if there is a differentiable structure, applying Chern–Weil Theory to the particular case of a line bundle, we can evaluate the first Chern class of a line bundle with a connection on a 2–dimensional submanifold by pulling back, i.e. restricting, the line bundle to the surface and integrating the curvature form of the connection.

4.3.1 Berry connection

Following Berry [9] we can use the connection provided by adiabatic transport. It was Berry's insight that this connection is indeed not always trivial and produces the so–called Berry phase as a possible monodromy. In the reinterpretation of Simon [11] this connection computes exactly the first Chern class of the line bundle L_i, which is the only obstruction for L_i and hence the monodromy to be trivial.

4.4 Topological charges

There are several ways to get a scalar charge which one can exploit. Since the Chern classes have even degree, they will always produce zero when paired with odd dimensional homology classes. Thus we have to ensure that we use even dimensional cycles to integrate over. (Here integration means pairing with the fundamental class).

Assume T is compact orientable potentially with boundary and that $T_{\deg}$ is in codimension at least 1; i.e. T is generically non–degenerate. We furthermore assume that $T_{\deg} \cap \partial T = \emptyset$. Then T_0 is an orientable manifold with boundary. Let N be a tubular neighborhood of $T_{\deg}$ in T. Then $B = T \setminus N$ is a compact sub–manifold with boundary $\partial B = \partial T \amalg \partial \bar{N}$ where $\partial \bar{N} = \bar{N} \setminus N$. If B has 2nd cohomology, we can pair the β_i and Q_c with suitable homology classes.

Assume that $T_{\deg}$ is a manifold with singularities. If the smooth part of $T_{\deg}$ is of codimension r then $\partial \bar{N}$ is an S^{r-1} bundle over the smooth part of $T_{\deg}$.

4.4.1 Even dimensional T

If B is even dimensional, we can integrate over B itself and consider $Q_B = \int_B Q_c(t_i)$, the full B charge.

If in particular B is two–dimensional, we obtain all the individual charges $Q_i := \int_B \beta_i$.

Following Simon [11] this if for instance the case for the quantum Hall effect. Here $T = T^2$ has no degenerate locus and we have that $B = T$ can carry non–trivial line bundles. Indeed the arguments of TKNN [10] establish the non–triviality of the corresponding line bundle.

4.4.2 Odd dimensional T with boundary

If T_0 is odd dimensional, we can restrict the L_i to the boundary of ∂T. Then the *boundary charge* is $\int_{\partial T} Q_c(t)|_{\partial T_0}$.

In the differentiable case, we represent Q_c by a closed form $\omega = d\phi$; strictly speaking this is a polynomial form. Then since B is odd dimensional, we have by Stokes' Theorem that $0 = \int_B \omega = \int_{\partial B} \phi = \int_{\partial T} \phi + \int_{\partial \bar{N}} \phi$.

$$\int_{\partial T} \phi = -\int_{\partial \bar{N}} \phi = \int_{-\partial \bar{N}} \phi \tag{7}$$

where $-\partial \bar{N}$ has the outward orientation viewed from $\bar{N}$. Else we just use the usual pairing between the corresponding homologies and cohomologies.

If the boundary is empty, then we have that $\int_{\partial \bar{N}} \phi = 0$.

4.4.3 Codimension 3 and local charges

If the smooth part $T^{\text{sm}}_{\text{deg}}$ of T_{deg} is of codimension 3 then we can restrict the L_i to the fiber $S^2 = S^2(p)$ over any point p of $T^{\text{sm}}_{\text{deg}}$. We call $\int_{S^2(p)} L_i|_{S^2}(p)$ the i–th local charge at p and $\int_{S^2(p)} Q_c|_{S^2}(p)$ the total local charge.

4.4.4 Isolated critical points in dimension 3

For *isolated* critical points of T_{deg} the local charges are just given by integrating over small spheres around these points. If T_{deg} consists only of isolated critical points, then formula (7) states that the boundary charge is the sum over the local charges. If moreover the boundary is empty, this means that the sum of all the local charges is 0. This is the case for the gyroid.

4.5 Probing with surfaces

In order to detect the K–theoretic charges, we can send them to cohomology using the Chern classes and then detect them by using embedded surfaces. Explicitly, if Σ is an oriented compact surface and $i:\Sigma \to T$ is an embedding, then

$$Q_{\Sigma,i} := \int_{\Sigma} i^* c_1(L_i) = \langle c_1(L_i), i_*([\Sigma])\rangle \tag{8}$$

where $\langle\ ,\ \rangle$ is the standard pairing between cohomology and homology. Notice that by the results of Thom [30] all second homology classes are of this type even over $\mathbb{Z}$. In general, one has to take at least $\mathbb{Q}$ coefficients to ensure that all these integrals determine the cohomology class uniquely.

4.5.1 Slicing

A slicing for T is a smooth codimension 1 foliation by compact oriented manifolds of T which has a global transverse section S and the leaves of the foliation generically do not intersect $T_{\deg}$. For this we need the Euler characteristic to be 0, which is in particular the case for all odd dimensional compact manifolds.

For $s \in S$ let T_s be the leaf of s and i_s be the inclusion, we can consider the pullback of C and consider

$$Q_s := \int_{T_s} i^* C \tag{9}$$

which is the total Chern class of the slice. An interesting situation arises if

(1) T_s generically does not intersect $T_{\deg}$
(2) Any component of $T_{\deg}$ is contained between some pair of slices. That is for a component $T' \subset T_{\deg}$ there are s_1, s_2 and an n–dimensional submanifold M'_T of T with boundaries, such that $M_{T'} \cap T_{\deg} = T_0$, and $\partial M_{T'} \cap T_{\deg} = \emptyset$ and $\partial M_{T'} = T_{s_1} - T_{s_2}$.

In this case, by using Stokes' Theorem we get that the total contribution of T'

$$\int_{N\cap M_{T'}} Q_s = Q_{s_1} - Q_{s_2} \tag{10}$$

Now (11) is a great tool to numerically find $T_{\deg}$. For this one just runs through the $s \in S$ and looks for jumps in Q_s.

4.5.2 T_{deg} of codimension 3

If T' is smooth then the total charge is

$$\int_{Tdeg}(\int_{S^2(p)} C|_{S^2}(p))dp = Q_{s_1} - Q_{s_2} \tag{11}$$

If we are in dimension 3 then codimension 3 means that the degenerate locus consists of only isolated critical points. Here the equation (11) simplifies to just a finite sum over the critical points.

If furthermore the critical points are A_1 singularities, see §5.1, then the jumps in the charge are from ± 1 to ∓ 1, as calculated in [11, 31] depending on if one calculates for the upper or lower band and the chosen orientation/parameterization.

4.5.3 3–dimensional torus models

If we have that $T = T^3$ the situation is especially nice. It is fibred by T^2s in any sprojections $S^1 \times S^1 \times S^1 \to S^1$. The inclusion of fibers, say in the three coordinate projections, actually generates the whole cohomology of T^3 which has non–vanishing 2nd cohomology $H^2(T^3) \simeq \mathbb{Z}^3$. In contrast to the two–torus where puncturing kills the 2nd cohomology a punctured three torus actually still has second cohomology. It is given explicitly in the proof of the theorem below. This is a main difference between graphene and the gyroid, see below. One has to be sure however, that the condition of generically not intersecting the degenerate locus is not violated. This is for instance the case for the D–surface, see below.

Theorem 4.8 *For a smooth variation with base T^3 with and only finitely many degenerate points, the slicing method corresponding to a generic projection completely determines the K–theoretic charges and hence the line bundles L_i up to isomorphism.*

Proof If there are m degenerate points p_i then pick a generic projection and let $z_1, \dots, z_m \in S^1$ be the images of the p_i. Let $t_1, \dots, t_m$ be points in between the z_i, that is one point per component of $S^1 \setminus \{p_i\}$. Consider the CW model of the torus, which has one 2–cell at height t_i and 3–cells in between and 0 and 1 cells accordingly. Then $T_0 = T \setminus \{p_i\}$ deformation retracts onto the 2–skeleton of this complex. And the homology $H_2(T_0)$ is generated by exactly the m two cells. Now the slicing method will give the paring with these two cells and as the Poincaré paring is non–degenerate, we the cohomology class of $c_1(L_i)$ is determined by these numbers and hence the line bundle up to isomorphism. □

Notice that the slicing only gives a finite set of numbers for each Eigenvalue, since the integral over the Chern–class is constant in the components $S^1 \setminus \{p_i\}$.

4.6 Topological Stability

Having non–vanishing topological charges produces topological stability. If we perturb the Hamiltonian slightly by adding a small perturbation term λH_1 and continuously vary λ starting at 0, then T_0 does not move much —for instance as a submanifold of $T \times R$, see §5.1. In particular, there will be no new singular points in T_0 for small perturbation. The Eigenbundles over T_0 also vary continuously and hence so do their Chern classes. Since these are defined over $\mathbb{Z}$ they are actually locally constant, so that all the non–vanishing charges, scalar, K-theoretic or cohomological, must be preserved.

5 Swallowtails and symmetries

5.1 Characteristic map and Swallowtails

In the commutative case, the locus X_{deg} has a nice characterization in terms of singularity theory, [7].

The key ingredient is embedding of X into $T \times \mathbb{R}$ and the characteristic map. Let $P(z,t) = det(zId - H(t)) = z^k + b_{k-1}(t)z^{k-1} + \cdots + b_0(t)$, let $P(z - \frac{b_{k-1}}{k}, z) = z^k + a_{k-2}(t)z^{k-2} + \cdots + a_0(t)$ and let g be the isomorphism on $T \times \mathbb{R}$ which sends (t,z) to $(t, z - \frac{b_{k-1}}{k})$. The coefficients $a_{k-2}(t), \dots, a_0(t)$ define a map $\Xi : T \to \mathbb{C}^{k-1}$ called the characteristic map. Identifying $\mathbb{C}^{k-1}$ with the base of the miniversal unfolding of the A_{k-1} singularity, we obtain the following generalization of [7]:

Theorem 5.1 *The branched cover $X \to B$ is equivalent via g to the pull back of the miniversal unfolding of the A_{k-1} singularity along the characteristic map Ξ.*

Moreover is the family of Hamiltonians is traceless, which is for example the case if $\bar{\Gamma}$ has no small loops —that is edges which are a loop at one vertex—, the cover is the pull–back on the nose.

Furthermore, if the graph is also simply laced, then $a_{k-1} = |E(\bar{\Gamma})|$ and the image of T is contained in that slice.

This means that if $\Sigma \subset \mathbb{C}^{k-1}$ is the discriminant locus or swallowtail, then $T_{\deg} = g^{-1}(\Xi^{-1}(\Sigma))$ and the fiber of π over a point t is exactly $g^{-1}\pi_A^{-1}(\Xi(t))$ where π_A is the projection of the miniversal unfolding. In other words the fibers over degenerate points are identified with the corresponding fibers over their image points in the swallowtail.

Using Grothendieck's characterization [32] of the swallowtail as stratified by lower order singularities obtained by deleting edges in the corresponding Dynkin diagram, we obtain:

Corollary 5.2 *The only possible types of singularities for $(\bar{\Gamma}, \rho)$ with traceless Hamiltonians in the spectrum are $(A_{r_1}, \dots, A_{r_s})$ with $\sum r_i \leq k - s$.*

Remark 5.3 Theorem 5.1 and the corollary above can be viewed as a more precise statement of what is commonly referred to as the von Neumann–Wigner theorem. Namely the expectation that the degenerate locus is of codimension 3. This is the case for the full family of Hermitian Hamiltonians as shown in [33]. In general the exact codimension depends on the whole family T and is given precisely as the preimage of Ξ. To be more precise locally it is the dimension of the intersection of the image under Ξ with the swallowtail and the dimension of the fiber.

Proposition 5.4 *In the maximal toric case increasing the number of links to arbitrarily high values, the codimension of the degenerate locus T_{deg} generically becomes $-\chi(\Gamma)$, so that the stable expected codimension of the critical locus is 1.*

Proof Since the domain of Ξ is compact, so is the image. Its size is limited by the coefficients of the Hamiltonian. The value of i,j–th entry under $\hat{\chi}$ is sharply bounded by l where l is the number of edges between v_i and v_j. As the number of edges grows this bound increases. This implies that the sharp bound on the coefficients a_i also increases. If this is large enough, the image of Ξ will fill out a bounded region of the complement of the swallowtail Σ over which the discriminant is positive. Then the boundary of the image given by a part of the swallowtail Σ will be of codimension 1 and of dimension $|V_\Gamma| - 2$. The generic dimension of the fiber will be $dim(T) - (|V_\Gamma| - 1)$. In total this gives the dimension of the critical locus as $1 - \chi(\Gamma) - |V_\Gamma| + 1 + |V_\Gamma| + 2 = -\chi(\Gamma)$. □

The test case of the triangular graph has been calculated in [26] which gives an example of the phenomenon described above.

5.2 Characterizing Dirac points

Physically very interesting singularities of X are conical singularities, which are also called Dirac points. In order to find these singularities, we considered the ambient space $T \times \mathbb{R}$ and the function $P : T \times \mathbb{R} \to \mathbb{R}$. As we argued in [7], Dirac points in the spectrum are isolated Morse singularities of P with signature $(+,-,\dots,-)$. That argument did not need the specifics of the geometric situation and hence generalizes.

Notice that a necessary condition from the above is that there is an A_1 singularity in the fiber. In addition one needs to check the signature.

5.3 Symmetries and the re–gauging groupoid [8]

5.3.1 General setup

Going back to the embedding of $\mathscr{B}_\Theta$ into $M_k(\mathbb{T}^n_\Theta)$ the relevant matrix representation depended on the choice of a rooted spanning tree (τ, v_0) and an order $<$ on the vertices. We will now fix that the first element in that order is given by the root. In [8] we showed that the re–gauging from $(\tau,<)$ to $(\tau',<')$ is given by conjugation by a unitary matrix $U_{\tau,<}^{\tau',<}$. These matrices are more complicated than just the permutation group and incorporate local gaugings. These are given by diagonal matrices with invertible elements in $\mathbb{T}_\Theta$ indexed by the vertices of the graph.

Moreover in this way, the automorphism group of Γ acts by re–gaugings. Namely, if $\phi \in Aut(\Gamma)$ then given $(\tau,<)$, the image of τ, $\phi(\tau)$, and the push forward of the order, $\phi_*(>)$, give rise a re–gauging by $U_{\tau,<}^{\phi(\tau),\phi_*(<)}$. Usually this action on a given Hamiltonian is not trivial, due to the fact that ρ need not be trivial.

All these observations directly generalize to the more general case of a groupoid representation $(\bar{\Gamma},\rho)$. In this case $\mathscr{B}_\Theta$ is replaced by $\mathscr{T}$. The arguments of [8] are not sensitive to the particular structure of $\mathbb{T}_\Theta$ and hence carry over to the more general situation. We summarize the logical steps here.

5.3.2 Re–gauging groupoid

The re–gaugings form a secondary groupoid, the re–gauging groupoid. Its objects are given by tuples $(\tau,<)$ and between any two objects there is a unique morphism $((\tau,<),(\tau',<'))$. There is a morphism λ to matrices with coefficients in $\mathscr{T}$ by sending $((\tau,<),(\tau',<'))$ to $U_{\tau,<}^{\tau',<}$. This morphism need not be a representation however, since

we are only guaranteed that $\lambda(g_1)\lambda(g_2)\lambda(g_1g_2)^{-1}$ is non–commutative 2–cocycle with values in $U(\mathscr{T})$, the unitary elements of $\mathscr{T}$. The reason for this is that under the identification given in § 3.4.5 the re–gauging basically corresponds to an isomorphism of $\pi_1(\bar{\Gamma}, v_0)$ with $\pi_1(\bar{\Gamma}, v_0')$ along a path, v_0 and v_0' being the roots of τ and τ' respectively. Concatenating the isomorphisms along these paths as above, we end up with an isomorphism under a loop; but this is precisely conjugation with an element of $\pi_1(\bar{\Gamma}, v_0)$. In the representation, this element becomes an element in $U(\mathscr{T})$.

5.3.3 Projective Groupoid Representations

In the commutative case the cocycle above gives rise to a central extension by $U(\mathscr{T})$ and the matrices $U_{\tau,<}^{\tau',<'}$ give a representation in $M_k(\mathscr{T})$ of the central extension.

Evaluating with a character $\hat{\chi}$, the extension becomes an extension by $U(1)$ and the matrices $\hat{\chi}(U_{\tau,<}^{\tau',<})$ form a projective representation of the groupoid in $M_k(\mathbb{C})$.

5.3.4 Stabilizer Groups, Lifts, Projective Actions and Group Extensions

If we have a fixed point, that is a Hamiltonian that is invariant under the action of non–trivial groupoid elements, then these form a *group* of re–gaugings. Technically the representation of stabilizer subgroupoid factors through the group given by identification of all objects in that groupoid to one point.

In order to find such a stabilizer group, we look for an automorphism of T which compensates the re–gauging by automorphisms of $\bar{\Gamma}$. That is given an automorphism ϕ of $\bar{\Gamma}$ let $\Phi_{\tau',<'}^{\tau,<}$ be the associated re–gauging. We then look for an automorphism $\Psi_{\tau',<'}^{\tau,<}$ of T such that

$$\hat{\chi}_t(\Phi_{\tau',<'}^{\tau,<}(H_{\tau,<})) = \hat{\chi}_{\Psi_{\tau',<'}^{\tau,<}(t)}(H_{\tau,<}) \tag{12}$$

This is done for one orbit of $(\tau, <)$ under $Aut(\bar{\Gamma})$. This tool is most effective is the graphs are completely symmetric, like the cases we considered.

If we find such a lift of the automorphism group $Aut(\bar{\Gamma}) \to Aut(T)$, then we can look for points of enhanced symmetry. If $t \in T$ has a non–trivial stabilizer group under this action of $Aut(\bar{\Gamma})$ then the matrix $\hat{\chi}_t(H_{\tau,<})$ has a non–trivial re–gauging fixed group. This action by conjugation yields a projective representation of the stabilizer group.

Given such a projective representation, we know that it is a representation of a central $U(1)$ extension of the stabilizer group. If the stabilizer group is finite, we would

furthermore like to find a smaller if possible finite group which already carries the representation. That is an extension of the stabilizer group by a finite group. For this one uses the theory of Schur multipliers.

The upshot is that the isotypical decomposition of the representation has to be commensurate with the Eigenspace decomposition of the Hamiltonian – for that particular value $t \in T$. Practically this means that on one hand if in the given representation there are irreps of dimension bigger than one, one can infer that there are degeneracies in the spectrum of at least these dimensions. On the other hand, the one dimensional isotypical components fix Eigenvectors and hence make it easy to find the Eigenvalues. In general of course one only has to diagonalize the Hamiltonian inside the isotypical summands.

In the geometric examples, we showed in [8] that all the degeneracies can be explained as being forced by these enhanced re–gauging symmetries.

6 Results and the conjectured NC/C Duality

Let us summarize our results for the different quantum wire networks, honeycomb, P, D and G. The basis are the results from [3, 7, 8, 26] and the new analysis for the topological charges.

6.1 The Honeycomb Lattice

6.1.1 The commutative case

In this case the space X is a double cover of the torus T^2 ramified at two points. These two points are A_1 singularities and Dirac points.

T_0 is T^2 with two points removed, so $H^2(T_0) = 0$ and so the all charges vanish and the two Dirac points are in general not topologically stable.

There has been an investigation of deformation directions which do not destroy these points [14]. In our setup this means the following: the characteristic map has its image in $[-9, 0]$ where the swallowtail for A_1 is the point 0. One only considers deformations which still have 0 in the image of the characteristic map.

At the Dirac points there is an enhanced symmetry which is Abelian, so it does not have any higher dimensional irreps, but the isotypical decomposition is fully decomposed and forces the double degeneracy at the Dirac points due form of the Hamiltonian.

6.1.2 Noncommutative case

Generically $\mathscr{B}_\Theta = \mathbb{T}^2_\Theta$. In order to give the degenerate points, let $-e_1 := (1,0), e_2 = \frac{1}{2}(1,\sqrt{3}), e_3 := \frac{1}{2}(1,-\sqrt{3})$ be the lattice vectors and $f_2 := e_2 - e_1 = \frac{1}{2}(-3,\sqrt{3})$, $f_3 := e_3 - e_1 = \frac{1}{2}(3,\sqrt{3})$ the period vectors of the honeycomb. The parameters we need are

(13)
$$\theta := \hat{\Theta}(f_2, f_3), \quad q := e^{2\pi i\theta} \quad \textit{and} \quad \phi = \hat{\Theta}(-e_1, e_2), \quad \chi := e^{i\pi\phi}, \textit{thus} \quad q = \bar{\chi}^6$$

where $\hat{\Theta}$ is the quadratic from corresponding to the B–field $B = 2\pi\hat{\Theta}$.

Theorem 6.1 *[3] The algebra $\mathscr{B}_\Theta$ is the full matrix algebra of $M_2(\mathbb{T}^2_\theta)$ except in the following finite list of cases*

(1) $q = 1$.

(2) $q = -1$ *and* $\chi^4 = 1$.

The precise algebras are given in [3]. We wish to point out that $q = \chi = 1$ is the commutative case and $q = -\chi = 1$ is isomorphic to the commutative case, while the other cases give non–commutative proper subalgebras of $M_2(\mathbb{T}^2_\theta)$.

6.2 The primitive cubic (P) case, and other Bravais cases

For the simple cubic lattice and any other Bravais lattice of rank k (P is the rank 3 case): if $\Theta \neq 0$ then $\mathscr{B}_\Theta$ is simply the noncommutative torus $\mathbb{T}^k_\Theta$ and if $\Theta = 0$ then this $\mathscr{B}_0$ is the C^* algebra of T^k. There are no degenerate points.

In the commutative case the cover $X \to T^k$ is trivial and so is the line bundle of Eigenvectors.

The analysis of [15] of the quantum Hall effect however suggests that there is a non–trivial noncommutative line bundle in the case of $k = 2$ for *non–zero B–field*. Furthermore, in this case there is a non–trivial bundle, not using the noncommutative geometry, but rather the Eigenfunctions constructed in [10] for the full Hilbert space $\mathscr{H}$. This is what is also considered in [11]. We will study this phenomenon in the gyroid and the other cases in the future.

6.3 The Diamond (D) case

6.3.1 The commutative case

In this case, we see that the algebra $\mathscr{B}_\Theta$ is a subalgebra of $M_2(C(T^3))$, where $C(T^3)$ is the C^* algebra of complex functions on the torus T^3.

The space X defined by $\mathscr{B}$ in the commutative case is a generically 2–fold cover of the 3–torus T^3 where the ramification locus T_{deg} is along three circles on T^3 given by the equations $\phi_i = \pi, \phi_j \equiv \phi_k + \pi \text{ mod } 2\pi$ with $\{i, j, k\} = \{1, 2, 3\}$. $T_{\text{deg}}\Xi^{-1}(0)$ is the inverse image —of the characteristic map— of the only singular points (the origin) of the miniversal unfolding of A_1. Thus the singularities are of type A_1 but they are not discrete, but rather pulled back to the entire T_{deg}, hence there are also no Dirac points.

One can show that $T_0 = T^3 \setminus T_{\text{deg}}$ contracts onto a 1–dimensional CW–complex and hence has $H^2(T_0) = 0$. Thus there are no non–vanishing topological charges associated to this geometry and no stability.

Analogous to the honeycomb case there are Abelian enhanced symmetries with 1–dimensional isotypical components, which force the double degeneracy in view of the structure of the Hamiltonian.

6.3.2 The non–commutative case

In the non–commutative case, we express our results in terms of parameters q_i and ξ_i defined as follows: Set $e_1 = \frac{1}{4}(1, 1, 1), e_2 = \frac{1}{4}(-1, -1, 1), e_3 = \frac{1}{4}(-1, 1, -1)$ for $B = 2\pi\Theta$ let

(14)

$$\Theta(-e_1, e_2) = \varphi_1 \quad \Theta(-e_1, e_3) = \varphi_2 \quad \Theta(e_2, e_3) = \varphi_3 \text{ and } \chi_i = e^{i\varphi_i} \text{ for } i = 1, 2, 3$$

There are three operators U, V, W, given explicitly in [26], which span $\mathbb{T}^3_\Theta$ and have commutation relations

$$UV = q_1 VU \quad UW = q_2 WU \quad VW = q_3 WV \tag{15}$$

where the q_i expressed in terms of the χ_i are:

$$q_1 = \bar{\chi}_1{}^2 \chi_2^2 \chi_3^2 \quad q_2 = \bar{\chi}_1{}^6 \bar{\chi}_2{}^2 \bar{\chi}_3{}^2 \quad q_3 = \bar{\chi}_1{}^2 \bar{\chi}_2{}^6 \chi_3^2 \tag{16}$$

Vice versa, fixing the values of the q_i fixes the χ_i up to eighth roots of unity:

$$\chi_1^8 = \bar{q}_1 \bar{q}_2 \quad \chi_2^8 = q_1 \bar{q}_3 \quad \chi_3^8 = q_1^2 \bar{q}_2 q_3 \tag{17}$$

Other useful relations are $q_2\bar{q}_3 = \bar{\chi}_1^4 \chi_2^4 \bar{\chi}_3^4$ and $q_2 q_3 = \bar{\chi}_1^8 \bar{\chi}_2^8$. the algebra $\mathscr{B}_\Theta$ is the *full* matrix algebra *except* in the following cases in which it is a proper subalgebra.

(1) $q_1 = q_2 = q_3 = 1$ (the special bosonic cases) and one of the following is true:
  (a) All $\chi_i^2 = 1$ then $\mathscr{B}_\Theta$ is isomorphic to the commutative algebra in the case of no magnetic field above.
  (b) Two of the $\chi_i^4 = -1$, the third one necessarily being equal to 1.

(2) If $q_i = -1$ (special fermionic cases) and $\chi_i^4 = 1$. This means that either
  (a) all $\chi_i^2 = -1$ or
  (b) only one of the $\chi_i^2 = -1$ the other two being 1.

(3) $\bar{q}_1 = q_2 = q_3 = \bar{\chi}_2^4$ and $\chi_1^2 = 1$ it follows that $\chi_2^4 = \chi_3^4$. This is a one parameter family.

(4) $q_1 = q_2 = q_3 = \bar{\chi}_1^4$ and $\chi_2^2 = 1$ it follows that $\chi_1^4 = \bar{\chi}_3^4$. This is a one parameter family.

(5) $q_1 = q_2 = \bar{q}_3 = \bar{\chi}_1^4$ and $\chi_1^2 = \bar{\chi}_2^2$. It follows that $\chi_3^4 = 1$. This is a one parameter family.

6.4 The Gyroid (G) case

6.4.1 The commutative case

For the gyroid, the commutative geometry if given by a generically unramified 4-fold cover of the three torus, see [3]. There are only 4 ramification points. This means that the locus is of real codimension 3 contrary to the D case where it was of codimension 2. Furthermore the degenerations are 3 branches coming together at 2 points —$(0,0,0)$ and (π,π,π)— and 2 pairs of branches coming together at the other two points —$(\frac{\pi}{2},\frac{\pi}{2},\frac{\pi}{2})$ and $(\frac{3\pi}{2},\frac{3\pi}{2},\frac{3\pi}{2})$. The latter furnish double Dirac points.

Using the characteristic map the first type of singular point corresponds to an A_2 singularity and the second type corresponds to the type (A_1,A_1) stratum of the swallowtail. All the inverse images have discrete fibers. There are two image points on the A_2 stratum each with one inverse image under Ξ and there is one point on the (A_1,A_1) stratum, with two inverse images.

All the A_1 singularities in the fibers are Dirac points. That is there are four of these points. Furthermore at all points there are enhanced symmetries by non–Abelian groups.

At $(0,0,0)$ the enhanced symmetry group is the symmetric group $\mathbb{S}_4$ —the full symmetry group of $\bar{\Gamma}$ which entirely lifts to $Aut(T^3)$— yielding one 1–dim irrep and one

3–dim irrep which forces the triple degeneracy. At (π,π,π) we have an *a priori* projective representation of $\mathbb{S}_4$, which we showed however to be equivalent to the standard representation of $\mathbb{S}_4$ and hence we again get one 1–dim irrep and one 3–dim irrep which forces the triple degeneracy. At the other two points things are really interesting. The stabilizer symmetry group is A_4 and it yields a projective representation which is carried by the double cover of A_4 aka. $2A_4$, 2T, the binary tetrahedral group or $SL(2,3)$. The representation decomposes into two 2–dim irreps forcing the two double degeneracies.

Notice that we essentially need a projective representation, since A_4 itself has no 2–dim irreps.

Now $T_{\deg}$ is the set of the four points above and $T_0 = T^3 \setminus T_{\deg}$ contracts onto a 2–dim CW complex with non–trivial second homology.

Thus there are K–theoretic and cohomological charges. This is the special case of dimension 3 with codimension 3 degenerate points and moreover we have a slicing of T^3 by the fiber bundle $T^3 \to T^2$ by any of the tree coordinate projections. In fact the homology is generated by any four slices which sit in between the 4 slices that contain the degenerate points. Pairing with these surfaces completely determines the Chern class of the line bundles and hence the line bundles up to isomorphism.

The relevant numerics were carries out in [13]. In accordance with the analytic calculations of [11, 31] the Dirac points yield jumps in the charge by ± 1 for the two bands that cross.

A new result is that the A_2 points yield jumps by $-2, 0, 2$ for the three bands that cross.

All these charges are topologically stable. Again an interesting note is that the A_2 points each split into four A_1 points in compliance with the jumps given above.

6.4.2 The non–commutative case

To state the results of [3] we use the bcc lattice vectors

$$g_1 = \frac{1}{2}(1,-1,1), \quad g_2 = \frac{1}{2}(-1,1,1), \quad g_3 = \frac{1}{2}(1,1,-1) \tag{18}$$

$$\theta_{12} = \frac{1}{2\pi} B \cdot (g_1 \times g_2), \quad \theta_{13} = \frac{1}{2\pi} B \cdot (g_1 \times g_3), \quad \theta_{23} = \frac{1}{2\pi} B \cdot (g_2 \times g_3)$$

$$\alpha_1 := e^{2\pi i \theta_{12}} \bar{\alpha}_2 := e^{2\pi i \theta_{13}} \alpha_3 := e^{2\pi i \theta_{23}}$$

$$\phi_1 = e^{\frac{\pi}{2}i\theta_{12}}, \quad \phi_2 = e^{\frac{\pi}{2}i\theta_{31}}, \quad \phi_3 = e^{\frac{\pi}{2}i\theta_{23}}, \quad \Phi = \phi_1\phi_2\phi_3$$

Classification Theorem.

(1) If $\Phi \neq 1$ or $\Phi = 1$ and at least one $\alpha_i \neq 1$ and all ϕ_i are different then $\mathscr{B}_\Theta = M_4(\mathbb{T}^3_\Theta)$.

(2) If $\phi_i = 1$ for all i then the algebra is the same as in the commutative case.

(3) In all other cases $\mathscr{B}$ is non–commutative and $\mathscr{B}_\Theta \subsetneq M_4(\mathbb{T}^3_\Theta)$.

6.5 Observation and conjecture

Looking at the cases above, we observe several regularities. First and foremost, there is agreement on the maximal dimension of the degenerate locus in T^k between the commutative and the non–commutative case. In the commutative case, this locus is $T_{\deg}$; in the non–commutative case, it is the values of the B–field, which is again parameterized by T^k, now via Θ, where the matrix algebra is not the full matrix algebra.

We conjecture that this is always the case.

There are several possible points of attack here. The first is through the symmetries: as we have seen, the re–gauging groupoid exists already in the non–commutative case. Another is to consider how, in the presence of a conserved topological charge, larger representations, such as A_2 in the gyroid case, break into smaller pieces. Using the slicing method described above, one can readily see how that happens under a deformation of the Hamiltonian in the commutative case. The question is whether the effect of non-commutativity is something similar.

Acknowledgments

RK thankfully acknowledges support from NSF DMS-0805881. BK thankfully acknowledges support from the NSF under the grant PHY-0969689. Any opinions, findings and conclusions or recommendations expressed in this material are those of the authors and do not necessarily reflect the views of the National Science Foundation. The authors also thank the organizers of the conference: “Noncommutative Algebraic Geometry and its Applications to Physics” in Leiden for an event that catalyzed new results and research directions. They also thank M. Marcolli for insightful discussions.

Parts of this work were completed when RK was visiting the IHES in Bures–sur–Yvette, the Max–Planck–Institute in Bonn and the University of Hamburg with a Humboldt fellowship. He gratefully acknowledges their support.

References

[1] V.N. Urade, T.C. Wei, M.P. Tate and H.W. Hillhouse. *Nanofabrication of double-Gyroid thin films.* Chem. Mat. 19, 4 (2007) 768-777

[2] S. Khlebnikov and H. W. Hillhouse, *Electronic Structure of Double-Gyroid Nanostructured Semiconductors: Perspectives for carrier multiplication solar cells*, Phys. Rev. B 80, 115316 (2009)

[3] R.M. Kaufmann, S. Khlebnikov, and B. Wehefritz–Kaufmann, *The geometry of the double gyroid wire network: quantum and classical*, Journal of Noncommutative Geometry 6, 623-664 (2012)

[4] J. Bellissard, *Gap labelling theorems for Schrödinger operators*, in: From number theory to physics (1992) 538–630

[5] A. Connes, *Noncommutative Geometry*. Academic Press, Inc., San Diego, CA, 1994.

[6] M. Marcolli and V. Mathai, *Towards the fractional quantum Hall effect: a noncommutative geometry perspective*, in: Noncommutative geometry and number theory: where arithmetic meets geometry, Caterina Consani, Matilde Marcolli (Eds.), Vieweg, Wiesbaden (2006) 235-263

[7] R.M. Kaufmann, S. Khlebnikov, and B. Wehefritz–Kaufmann, *Singularities, swallowtails and Dirac points. An analysis for families of Hamiltonians and applications to wire networks, especially the Gyroid*. Annals of Physics 327, 2865 (2012)

[8] R.M. Kaufmann, S. Khlebnikov, and B. Wehefritz–Kaufmann, *Re-gauging groupoid, symmetries and degeneracies for Graph Hamiltonians and applications to the Gyroid wire network*. DESY preprint 12-133, preprint arXiv:1208.3266, submitted.

[9] M. V. Berry, *Quantum phase factors accompanying adiabatic changes*, Proc. R. Soc. Lond. A 392, 45–57 (1984)

[10] D.J. Thouless, M. Kohmoto, M.P. Nightingale and M. den Nijs, *Quantized Hall Conductance in a Two–Dimensional Periodic Potential*, Phys. Rev. Lett. 49, 405–408 (1982)

[11] B. Simon, *Holonomy, The Quantum Adiabatic Theorem, and Berry's Phase*, Phys. Rev. Lett. 51, 2167–2170 (1983)

[12] G. Xu, H. Weng, Z. Wang, X. Dai, and Z. Fang, *Chern Semimetal and the Quantized Anomalous Hall Effect in* $HgCr_2Se_4$, Phys. Rev. Lett. 107, 186806 (2011).

[13] R.M. Kaufmann, S. Khlebnikov, and B. Wehefritz–Kaufmann, *Topologically stable Dirac points in a three-dimensional supercrystal*. In preparation.

[14] C.F. Fefferman, M.I. Weinstein, *Honeycomb Lattice Potentials and Dirac Points*, preprint arXiv:1202.3839

[15] J. Bellissard, A. van Elst and H. Schulz-Baldes, *The noncommutative geometry of the quantum Hall effect. Topology and physics*, J. Math. Phys. 35 (1994) 5373–5451

[16] G. De Nittis and G. Landi, *Topological aspects of generalized Harper operators*, To appear in: The Eight International Conference on Progress in Theoretical Physics, Mentouri University, Constantine, Algeria, October 2011; Conference proceedings of the AIP, edited by N. Mebarki and J. Mimouni; preprint arXiv:1202.0902v1

[17] V. Ya. Demikhovskii and D. V. Khomitskiy, *Quantum Hall effect in p–type heterojunction with a lateral surface superlattice*, Phys. Rev. B 68 (2003) 165301

[18] N. Goldman and P. Gaspard, *Quantum graphs and the integer quantum Hall effect*, Phys. Rev B 77 (2008) 024302

[19] B. A. Bernevig, T. L. Hughes, S. Raghu and D. P. Arovas, *Theory of the Three–Dimensional Quantum Hall Effect in Graphite*, Phys. Rev. Lett. 99 (2007) 146804

[20] M. Koshino, H. Aoki, K. Kuroki, S. Kagoshima and T. Osada, *Hofstadter Butterfly and Integer Quantum Hall Effect in Three Dimensions*, Phys. Rev. Lett. 86 (2001) 1062

[21] J. Goryo and M. Kohmoto, *Berry Phase and Quantized Hall Effect in Three–Dimension*, J. Soc. Jpn. 71 (2002) 1403

[22] K. Grosse-Brauckmann and M. Wohlgemuth, *The gyroid is embedded and has constant mean curvature companions*, Calc. Var. Partial Differential Equations 4 (1996) 499

[23] A.H. Schoen, *Infinite periodic minimal surfaces without self-intersections*, NASA Technical Note No. TN D -5541 (1970)

[24] C. A. Lambert, L. H. Radzilowski, E. L. Thomas, *Triply Periodic Level Surfaces as Models for Cubic Tricontinous Block Copolymer Morphologies*, Philos. Transactions: Mathematical, Physical and Engineering Sciences, Vol. 354, No 1715, Curved Surfaces in Chemical Structure (1996) 2009–2023

[25] D. A. Hajduk et. al., *The gyroid - a new equilibrium morphology in weakly segregated diblock copolymers* Macromolecules 27 (1994) 4063–4075.

[26] R.M. Kaufmann, S. Khlebnikov, and B. Wehefritz–Kaufmann, *The noncommutative geometry of wire networks from triply periodic surfaces*, Journal of Physics: Conf. Ser. 343 (2012), 012054

[27] A. H. Castro Neto, F. Guinea, N. M. R. Peres, K. S. Novoselov, and A. K. Geim, *The electronic properties of graphene*, Rev. Mod. Phys. 81, 109 (2009)

[28] P.G. Harper, *Single band motion of conduction electrons in a uniform magnetic field*, Proc. Phys. Soc. London A68 (1955), 874–878

[29] G. Panati, H. Spohn and S. Teufel, *Effective dynamics for Bloch electrons: Peierls substitution and beyond*, Comm. Math. Phys. 242 (2003) 547-578

[30] R. Thom. *Sous-variétés et classes d'homologie des variétés différentiables. II. Résultats et applications.* C. R. Acad. Sci. Paris 236, (1953). 573–575

[31] K. Grove and G. K. Pedersen, *Diagonalizing Matrices over C(X)*, J. Funct. Anal. 59, 65–89 (1984)

[32] M. Demazure, *Classification des germs à point critique isolé et à nombres de modules 0 ou 1 (d'après Arnol'd)*. Séminaire Bourbaki, 26e année, Vol. 1973/74 Exp. No 443, pp. 124-142, Lect. Notes Math. 431. Springer, Berlin 1975

[33] J. von Neumann and E. Wigner, *Über das Verhalten von Eigenwerten bei adiabatischen Prozessen*, Z. Phys. 30, 467 (1929)

Department of Mathematics, Purdue University, West Lafayette, IN 47907

Department of Physics, Purdue University, West Lafayette, IN 47907

Department of Mathematics and Department of Physics, Purdue University, West Lafayette, IN 47907

rkaufman@math.purdue.edu, skhleb@physics.purdue.edu,
ebkaufma@math.purdue.edu